BVI Observations of the Eclipsing Binary XZ Andromedae at the EKU Observatory

Marco Ciocca
Department of Physics, Geosciences, and Astronomy, Eastern Kentucky University, Richmond, KY 40475; marco.ciocca@eku.edu

Received January 23, 2022; revised April 4, 2022; accepted April 5, 2022

Abstract The eclipsing binary XZ Andromedae has been the subject of many observing campaigns, due to variability of its orbital period and the interesting mechanisms causing the change. We therefore observed this star during the period October–November 2021. We determined the current orbital period (P = 1.357308 (18) d), and using transformed standard BVI magnitudes, constructed a model of the eclipsing binary using the PHOEBE (Physics of Eclipsing Binaries) and Binary Maker 3 software packages to compare with results from previous studies. The model that best fit the data suggests that XZ And is a semidetached system with the secondary filling the Roche Lobe. The parameters fit of the primary (T_1 = 9393 K, mass M_1 = 2.1 solar masses, and radius R_1 = 2.2 solar radii) are indicative of a A1V main sequence star, while the secondary's parameters (T_2 = 5334, M_2 = 1.02, and R_2 = 2.40) point to a star in a more advanced evolutionary status.

1. Introduction

XZ And, R.A. = $01^h\ 56^m\ 51.52^s$, Dec. +42° 06' 02.2" (J 2000) (see Figure 1) is an eclipsing variable of the Algol type, that is, a more evolved, larger and cooler star with a hotter, younger companion. There is likelihood of mass transfer under these conditions and the ultimate evolution of the system will be one of a white dwarf orbiting the younger companion.

XZ And has been the subject of many observing campaigns, aiming at determining the eclipse period, its variation over time, and the mechanisms responsible for its variation. It was first reported as variable by Shapley (1923) with many other attempts at determination since then.

Blitzstein (1950, 1954) described the binary as a primary of spectral type A0 with a secondary of spectral type G4. Blitzstein (1954) reached the conclusion that the light between eclipses was not constant, thus suggesting a semidetached system, that the primary eclipse was due to occultation (this is an important aspect of our analysis), and that the depth and duration of the observed secondary eclipse could not be reconciled with the calculated light curve. Blitzstein provided two possible explanations: that the secondary eclipse is wider than the primary due to an elliptical orbit or that (verbatim) "the light in secondary eclipse is not that produced by an ordinary eclipse but is modified by rings or streams of gas."

Blitzstein observations were unfiltered. Reinhart (1967) performed a two-color photoelectric measurement and determined that both eclipses have the same duration and therefore eliminated the possibility of an elliptical orbit. Giuricin *et al.* (1980) concurred with the determination of the primary as A0 and concluded that the secondary instead be a G5. Demircan *et al.* (1995) performed another study on the period variation of XZ And (again identified as an evolved Algol system) by using additional data.

Demircan *et al.* determined that the Observed – Computed (O–C) diagram formed by the times of minimum light (ToM), and the orbital period of the system, could be explained in terms of the beat effect of two (or possibly three) cyclic variations differing in periods (P_1 = 137.5 yr, P_2 = 36.8 yr, and P_3 = 11.2 yr) and amplitudes. They examined three possible explanatory mechanisms: apsidal motion of the slightly elliptical orbit, light time effect due to additional objects in the system, and the period modulation due to magnetic activity cycle of cool secondary component star (Applegate 1989, 1992). They rejected the possibility of apsidal motion effect on the period variation, while they thought P_3 could be related to the cyclic magnetic activity of the secondary component. The third-body hypothesis required one or two under-luminous stars (with total mass of about 3 solar masses $M_\odot$) around the system. Their reported

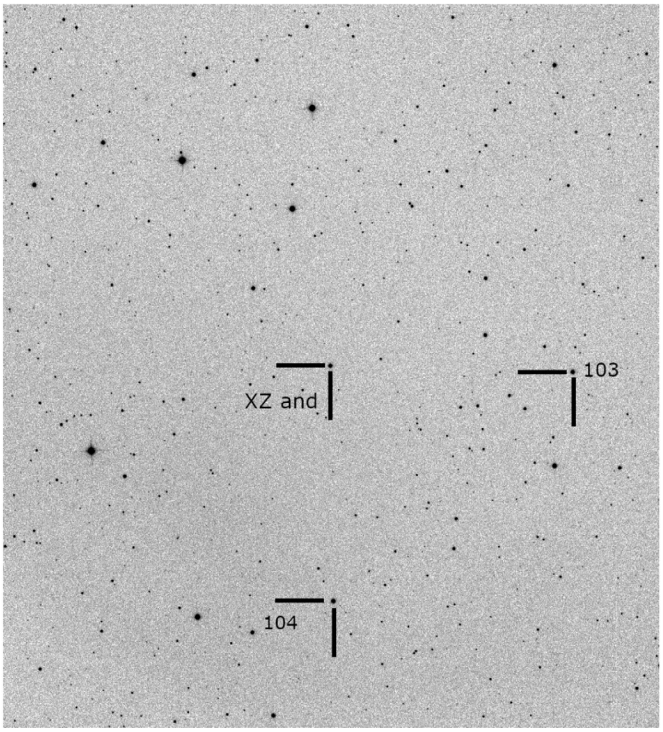

Figure 1. CCD frames (I_c Filter, 10 s integration time) showing the target star, comparison star, and check star. Star 104 (see Table 2 for its AUID designation) is the check star for the differential photometry of XZ And using VPHOT, while Star 103 is the comparison star. Scale: 1.90 arcseconds/pixel. Size (pixels): 1365 × 1365. Angular Size: 0°43'14" × 0°43'14". Position Angle (top of image): 86° 31' from north through east.

O–C diagram shows a good agreement with the third-body hypothesis.

2. Observations

2.1. Facilities

Eastern Kentucky University (EKU) Observatory has been described previously in Ciocca (2013). The telescope, however, is now an imaging Dall-Kirkham truss 17-inch telescope (IDK 17 from Planewave), with a Paramount ME II mount from Software Bisque. The instrument package now consists of a FLI 16803 Proline CCD, which has an array of 4096 × 4096 pixels, with 9-µm pixels, and is Anti-Blooming (ABG). The combination camera-telescope results in a field of view of 43 × 43 arcminutes, with an image scale of 1.90 arcsec/pixel when binning 3 × 3.

2.2. Telescope transformation parameters

We measured the transformation coefficients of the new scope-camera combination, as this allows converting the raw instrumental magnitudes to standard magnitudes, thus making comparisons with other measurements possible. This is done by using the software tools Transform Generator TG (Myers 2014) and Transform Applier TA (Silvis 2015). TG and TA made the process much simpler (Ciocca 2016). Recently, TA has been integrated with the online photometry software VPHOT, also provided by AAVSO (AAVSO 2012). We generated the transformation parameters by imaging the standard field NGC 7790 (one of the suggested star fields in TG) during October 2021.

The transformation parameters for our BVR$_c$I$_c$ filter set (Table 1) show a system close to the "ideal" case, as all the Color Index coefficients are approximately equal to 1 and the Filter Band Coefficients are near zero.

Table 1. Transformation parameters for the EKU observatory (November 2021).

Transformation Parameters	*Value and Uncertainties*
TBV	1.029 ± 0.016
TBR	1.021 ± 0.015
TBI	1.07 ± 0.010
TRI	0.98 ± 0.012
TVI	0.996 ± 0.01
TB_BV	0.008 ± 0.023
TB_BR	0.005 ± 0.015
TB_BI	0.005 ± 0.011
TV_BV	–0.02 ± 0.014
TV_VR	–0.035 ± 0.0024
TR_VR	–0.043 ± 0.018
TR_RI	–0.045 ± 0.022
TI_RI	–0.034 ± 0.023
TV_VI	–0.018 ± 0.015
TI_VI	–0.015 ± 0.011
TR_VI	–0.023 ± 0.01

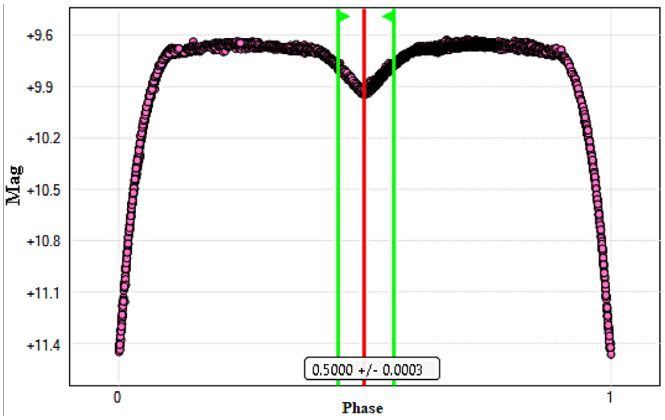

Figure 2. Phase plot of the transformed I$_c$ magnitudes (red dots). The green lines are used by Peranso to demark the data used to determine the time of minimum of the secondary eclipse. The minimum is at the red line.

3. Data Analysis

3.1. Orbital period determination

From October 11 to November 19, 2021, we observed XZ And via Johnson-Cousins BVI$_c$ filters. Data were not collected with R$_c$ as the standard stars available for the chart used (AAVSO chart X27525ALU, see also Figure 1) did not have any R$_c$ photometry available (see Table 2). Even though we had more standard stars available in the field of view, we limited the VPHOT sequence to one check and one comparison stars as to be able to use the Transform Applier routine, which is not yet capable of applying transform coefficient to ensemble photometry (see Figure 1 and Table 2).

Calibration of the CCD frames was done using PixInsight (Pleiades Astrophoto 2022) while plate solving was performed using The Sky X (Software Bisque 2018). The frames were then uploaded to, and the photometric results generated by VPHOT using the sequence shown in Table 2. After the differential photometry was complete, we uploaded the resulting observation files to the Transform Applier in VPHOT. This generated transformed magnitudes of XZ And.

We analyzed the transformed magnitudes via Peranso (Vanmunster 2013). This allowed us the determination of the orbital period and the generation of phase diagrams, with one example shown in Figure 2.

The period determined using data we collected between October and November 2021 is T = 1.357308 ± 0.000018 d, in good agreement to the period reported by the AAVSO International Variable Star Index (VSX; Watson *et al.* 2014). The uncertainty quoted in our determination (0.000018 d = 1.56 s) is

Table 2. Sequence stars used (AAVSO chart C27525ALU).

AUID	*R.A. (2000)* *h m s*	*Dec. (2000)* *° ′ ″*	*Label*	*B*	*V*	*I$_c$*	*Comments*
000-BBD-311	01 55 46.68	+42 05 26.0	104	11.417 (0.1133)	10.447 (0.075)	8.319 (0.153)	Check Star
000-BBD-332	01 56 45.66	+42 18 26.2	103	10.861 (0.110)	10.346 (0.079)	9.596 (0.170)	Comp. Star

simply the standard error of the mean of the values obtained in Peranso for each filter and does not reflect the base line uncertainty of the computer time, which is less than 0.2 sec / day (we use time calibration routines). In Figure 2, the phase plot generated by Peranso, using the determined orbital period, shows the location of the secondary minimum. This occurs at phase 0.5000 ± 0.0003, consistent with a purely circular orbit.

3.2. Time of Minimum (ToM), O–C, and period variability

Yang (2013) published an extensive work on XZ And, in which ToM from several sources and several ToM measured directly by that author, were used to build a more extensive O–C diagram, and compare it with a new model. These are the conclusions: the O–C graph showed a parabolic trend with a quasi-cyclic variation, with a time period of P_{mod} = 32.30 ± 0.06 yr and amplitude A = 0.0368 ± 0.0008 day, respectively. The model reproduced the data very effectively (see Figure 2 in Yang's paper).

We constructed an O–C diagram as well, in which we used exclusively the ToM we were able to determine using the CCD data available in the AAVSO International Database (Table 3). Most of the data in the database use the Johnson V filter. Our own V data are in the database as well, but we also have included our own Johnson B and Cousins I filters data. All the determinations are of the primary eclipse.

We used as epoch the first ToM we measured in the AAVSO database, and the period determined analyzing all the CCD data available in the database. We have: epoch = 2450430.6020 (25) JD and period = 1.357290 (1) d. The resulting O–C diagram is shown in Figure 3.

It is noteworthy to indicate that, by using the CCD data (covering the period December 1996–2021) in the AAVSO International Database, we obtained (using Peranso) the period shown above to plot the O–C diagram. If we limit the data to more recent dates (December 2015–2021), the period (P) obtained is instead P = 1.357299 (2). This appears consistent with an overall lengthening of the orbital period of XZ And, and further reflected in our own determination (with October–December 2021 data, approximately 30 cycles only) of P = 1.357308 (18) d.

By fitting the last 1,000 cycles of our O–C diagram with linear fit (Figure 4), we obtained the correction to the period and Epoch used in the generation of the diagram, resulting in a new epoch = 2459525.797977 JD and new eriod P = 1.3573008 d. These results are in agreement with Bob Nelson's analysis of XZ And (Southwest Research Inst. 2022). Nelson used a much larger data set, with over 1,100 ToM determinations.

Table 3. Time of Minima (TOM) for XZ And determined using CCD data in the AAVSO International Database.

HJD –240000	*Uncertainty (d)*	*Filter*	*HJD –240000*	*Uncertainty (d)*	*Filter*
50430.6020	0.002514	V	58050.4840	0.000051	V
51486.6005	0.002190	V	58058.6270	0.000183	V
53591.7900	0.001168	V	58073.5570	0.000053	V
53769.5960	0.000108	V	58100.7047	0.000076	B
54107.5660	0.000079	I	58100.7050	0.000108	I
54476.7510	0.001697	V	58100.7050	0.000173	V
54799.7890	0.000623	V	58100.7053	0.000181	B
54833.7200	0.000091	V	58111.5640	0.000058	V
54863.5800	0.000262	V	58374.8800	0.000043	V
55084.8178	0.000037	V	58392.5250	0.000067	V
55084.8180	0.000450	V	58396.5970	0.000049	V
55239.5490	0.000410	V	58415.6000	0.000106	V
55486.5740	0.000303	V	58456.3160	0.003142	V
55490.6460	0.000058	V	58464.4600	0.000056	V
55836.7520	0.000060	V	58479.3900	0.000080	V
55938.5470	0.000164	V	58494.3200	0.000054	V
56163.8550	0.001215	V	58712.8490	0.000058	V
56520.8210	0.000077	V	58825.5020	0.000095	V
56603.6150	0.000090	V	59130.8970	0.000070	V
56862.8560	0.001062	V	59167.5440	0.000085	V
57321.6200	0.000206	V	59186.5460	0.000077	V
57336.5500	0.000071	V	59426.7870	0.000117	V
57355.5520	0.000120	V	59498.7240	0.000469	I
57359.6240	0.000596	V	59498.7240	0.000549	V
57633.7960	0.000261	V	59498.7244	0.000515	B
57644.6560	0.001982	V	59506.8680	0.000342	I
57705.7320	0.000204	V	59506.8680	0.000398	V
57705.7330	0.001119	B	59506.8682	0.000394	B
57709.8040	0.000342	V	59509.5820	0.000265	I
57709.8049	0.000399	B	59509.5827	0.000454	B
57712.5180	0.001436	V	59509.5830	0.000351	V
57712.5200	0.000399	B	59524.5120	0.000529	V
57714.5560	0.001433	V	59524.5125	0.000380	B
57724.7378	0.000075	V	59524.5130	0.000416	I
57754.5940	0.000113	V	59525.8702	0.000278	B
58043.6990	0.000085	V	59525.8710	0.000487	I
58047.7710	0.000254	V	59525.8710	0.000203	V

4. Modeling using PHOEBE and Binary Maker 3

Many other authors—Manzoori (2016), Yang (2013), Demircan *et al.* (1995), Giuricin *et al.* (1980)—have solved the light curves using the WD code, from Wilson and Devinney (1971) and Wilson and Van Hamme (2014).

In this work, we used PHOEBE 0.32a (Legacy version, released in 2017) and followed, initially, a step-by-step manual by Zasche (2016), written for version 0.31. The 0.32a version of PHOEBE is also based on the WD code but has been updated with Castelli and Kurucs (2004) model atmospheres and has a built-in table of limb darkening (dated 2010). The results of the fit are in Tables 4 and 5. Manzoori (2016) used PHOEBE 0.31.

After attempting some of the other choices (detached Binary, double contact etc.) with poor results, we modeled XZ And as a semi-detached system with the secondary filling its Roche lobe, a configuration typical for Algol-type eclipsing binaries (see Figure 5 for a 3-D model of the star) and used by both Yang (2013) and Manzoori (2016). The latter had access to radial velocity data and therefore was able to determine the mass ratio ($q = M_2 / M_1$) and the semimajor axis of the system A directly. We used those determinations, q = 0.485 ± 0.02 and A = 7.53 ± 0.21 in solar Radii respectively, as fixed input values for PHOEBE.

The primary spectral characterization of XZ And is reported as A1V by Manzoori (2016), based on the determination of Halbedel (1984). We therefore set the initial temperature of the Primary as 9500 K, as per Manzoori (2016), but we left this parameter as free for PHOEBE to fit. After many iterations, the fit settled on T_1 = 9393 K.

In the literature there is a large variation of the temperature of the cooler companion (and ensuing spectral class) ranging

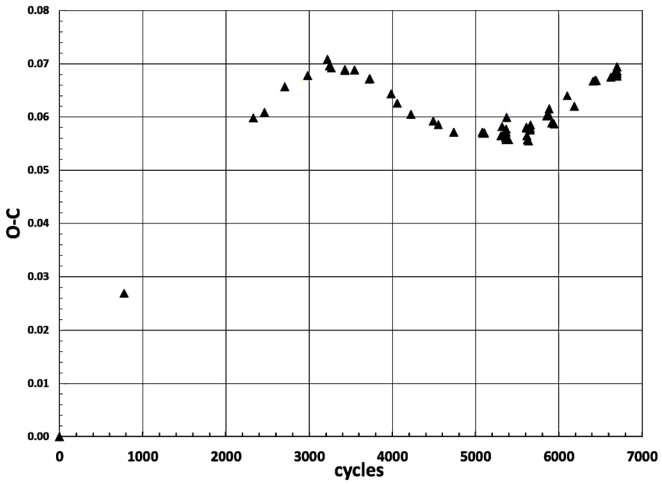

Figure 3. O–C diagram with Times of Minima from the AAVSO International Database.

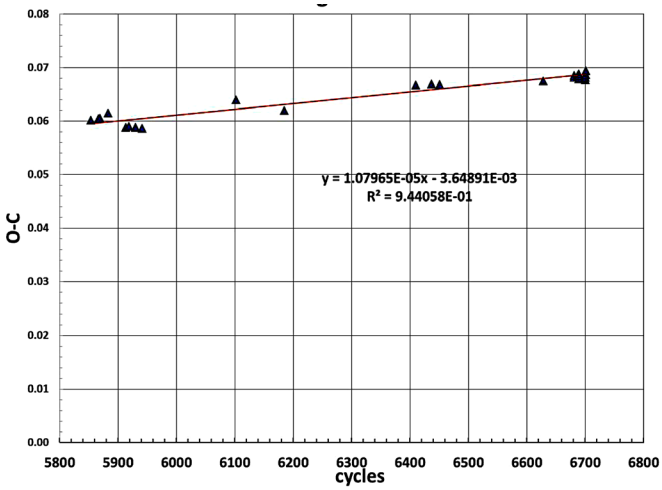

Figure 4. O–C diagram of the last 1,000 cycles to obtain correction to the period and the new epoch for XZ And.

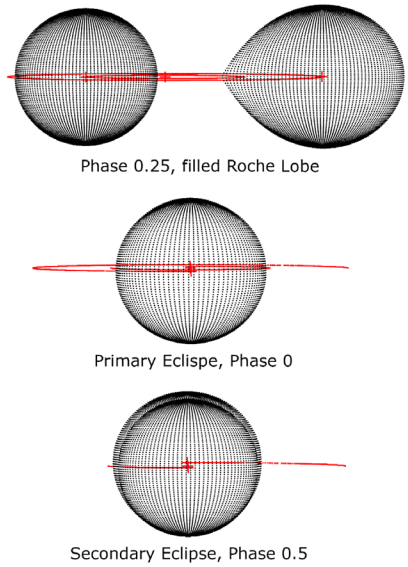

Figure 5. XZ And 3-d model generated by Binary Maker 3 using the parameters found in PHOEBE, showing the secondary filling its Roche Lobe, the Primary Eclipse, and the Secondary Eclipse.

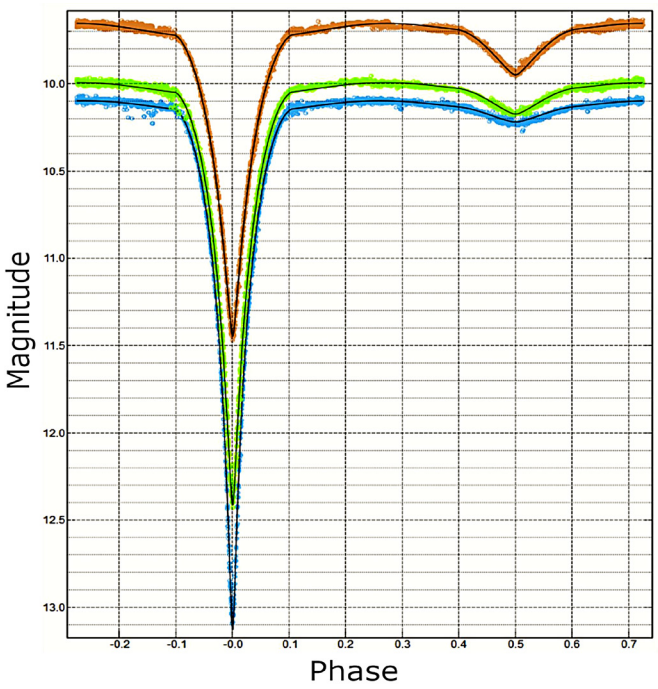

Figure 6. BVI observational magnitudes of XZ And with fit obtained using PHOEBE. Top to Bottom, I_c, V, and B filters. The fit is the solid line. Notice the differing depths of the primary and secondary eclipses as mentioned in the text.

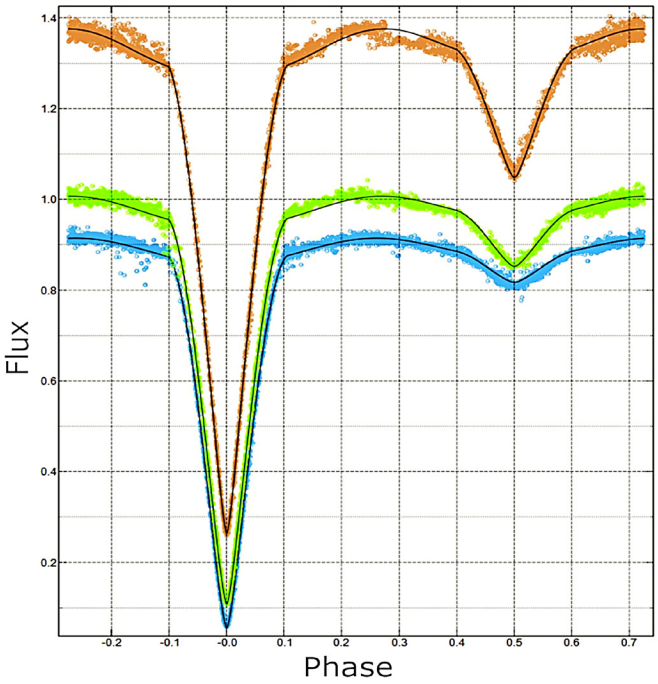

Figure 7. BVI observational fluxes of XZ And with fit obtained using PHOEBE. Top to Bottom, I_c, V, and B filters. The fit is the solid line. Notice the differing depths of the primary and secondary eclipses as mentioned in the text.

Table 4. Fit Parameters used and determined in PHOEBE.

Parameters	*This work*	*Manzoori (2016)*	*Yang (2013)*
T_0 HJD	2459498.723672	2423977.1915	1.424152.2546
P d	1.357308	1.357285	1.35727963
i °	88.34 ± .02	89.80 ± 0.04	88.4 ± 0.13
T_1 (K)	9393 ± 13	9500	9400
T_2 (K)	5337 ± 6	5100 ± 246	5094 ± 4
Ωı	4.09 ± 0.01	4.55 ± 0.12	3.8347 ± 0.0024
Ω_2	2.85 ± 0.01	2.84	2.8255
q	0.485 ± 0.02 (Note 1)	0.485 ± 0.02	0.474 ± 0.0003
$(L_1/(L_1+L_2))$ B	0.945 ± 0.01	0.869 ± 0.02 (Note 2)	0.9609 ± 0.0004
$(L_1/(L_1+L_2))$ V	0.891 ± 0.01	—	0.9198 ± 0.0005
$(L_1/(L_1+L_2))$ I	0.793 ± 0.01	—	0.8702 ± 0.0006 (Note 3)
$(L_2/(L_1+L_2))$ B	0.055 ± .01	0.1310 ± 0.003 (Note 2)	—
$(L_2/(L_1+L_2))$ V	0.109 ± 0.01	—	—
$(L_2/(L_1+L_2))$ I	0.207 ± 0.01	—	—
(l_3) B	0.0032 ± 0.0005	0.004 ± 0.002 (Note 2)	—
(l_3) V	0.003 ± 0.001	—	—
(l_3) I	0.003 ± 0.001	—	—
e	0	$0.001 \pm 2.170 \times 10^{-4}$	—
F_1	1.980 ± 0.009	3.20 ± 0.011	—
F_2	1	1	—
(X_1) B	0.560	0.621 (Note 2)	Note 4
(X_2) B	0.861	0.622 (Note 2)	—
(X_1) V	0.476	—	—
(X_2) V	0.717	—	—
(X_1) I	0.315	—	—
(X_2) I	0.524	—	—
Number of Points	B = 3194, V = 2465, I = 3225	10277	B = 994, V = 989, R = 992
ALB 1	1.0	1.0	—
ALB 2	0.5	0.5	—
GBR 1	1.0	1.0	—
GBR 2	0.32	0.32	—
r_1 (pole)	0.276 ± 0.001	—	0.2958 ± 0.0002
r_1 (side)	0.297 ± 0.001	—	0.3018 ± 0.0002
r_1 (point)	0.306 ± 0.001	—	0.3102 ± 0.0003
r_1 (back)	0.303 ± 0.001	—	0.3070 ± 0.0002

Notes 1. Value adopted from Manzoori (2016). 2. Manzoori's data were obtained with a broadband filter (400–700 nm). 3. Yang used the R passband here. 4. Yang adopted a different Limb Darkening Law.

Table 5. Physical and orbital parameters, of XZ And.

Parameter	*This Work*	*Manzoori (2016)*	*Yang (2013)*
Semi-major axis A (in solar radii)	7.53 ± 0.21 (adopted from Manzoori)	7.53 ± 0.21	8.20
$M_{1\odot}$	2.10 ± 0.01	2.102 ± 0.010	2.15
$M_{2\odot}$	1.02 ± 0.01	1.017 ± 0.020	1.02
$R_{1\odot}$	2.20 ± 0.01	2.288 ± 0.042	2.30
$R_{2\odot}$	2.40 ± 0.01	2.401 ± 0.053	2.59

from 5094 K (Yang 2013) to 5500 K (Demircan *et al.* 1995) to 5470 K (Giuricin *et al.* 1980). In the work on XZ And by Manzoori (2016), the author's fit provided a value of 5100 ± 246 K.

In our data there are five primary eclipses. The primary eclipse has been described as an occultation (Blitzstein 1954), in which the cooler secondary completely obscures the hot primary. Considering also that the inclination of the system, as described by all previous published works as approximately 88–89 degrees, we assumed that during a primary eclipse the light is coming solely from the secondary star. We therefore used the color Index B–V at the minima of the light curve at the primary eclipse to give us an initial estimate of the temperature of the cooler star.

The weighted average of the B–V term at the minimum of all the primary eclipses in our data set is B–V = 0.67 ± 0.01 mag.

Making use of Ballesteros (2012), of the Sekiguchi and Fukugita (2000) fit, of the Galactic Dust Reddening and Extinction tool (https://irsa.ipac.caltech.edu/applications/DUST/), based on the work by Schlafly and Finkbeiner (2011), and other approximate formulae (Imaging the Universe Lab Manual (University of Iowa 2017)), we obtained an average value for T_{eff} of 5471 ± 100 K for the secondary. This is consistent with the spectral determination of the secondary as G5IV by Demircan *et al.* (1995). We therefore set this temperature as a starting point for the fit by PHOEBE, but we kept it too as a free parameter. For each PHOEBE iteration we interpolated the limb darkening coefficients tables available in PHOEBE to match

the temperatures determination of the primary and secondary. After several cycles of this approach, and observing very small changes of those parameters, we set T_{eff1} and T_{eff2} at the values shown in Table 5. Therefore, the limb darkening coefficient shown correspond to these temperatures.

Demircan *et al.* (1995) and Manzoori (2016) accounted, in their solution, for the presence of a third body. Because of this, we also had PHOEBE fit the third light parameter, l_3, in the three passband, B, V, and I. The values we obtained are fairly small and converged to the values shown after many iterations.

Manzoori also obtained better results by modeling the rotation of the primary as non-synchronous with the orbital period. We followed suit and indeed obtained a better fit if we allowed the corresponding parameter F_1 to be fit by PHOEBE as well. We obtained the best results with $F_1 = 1.970 \pm 0.009$. Manzoori, with a much larger data set spanning a much larger period of time, obtained a best fit with F1 = 3.20 ± 0.011.

Another free parameter we used was the inclination i of the plane of the binary system.

Given the chosen temperatures (even if set as free parameters initially), we treated the primary as having a radiative atmosphere, while the secondary as convective. This was reflected in our choosing the albedo and gravity brightening parameters (ALB and GR) for the Primary as ALB1 = 1 and GR1 = 0.5 for the primary, while for the secondary we had ALB2 = 0.5 and GR2 = 0.32 respectively, which are the standard choices.

PHOEBE's fit is excellent, and it is shown in Figure 6 (Magnitudes) and Figure 7 (Fluxes), with the observations in the three filters. These phased plots use the orbital period and epoch, generated with Peranso analysis, of the data we collected during October–November 2021 (HJD time = 2459498.723672, and T = 1.357308 d respectively), as opposed to the period determined over the last 1,000 cycles as shown in section 3.2 using the last 1,000 cycles of the O–C diagram.

The light change in secondary eclipse, when observed through I_c filter, appears deeper in than the one through the V filter which, in turn, is also deeper that the one in B (see Figure 6 and 7). This suggests that when the secondary is behind the primary star, there is little light lost at the B (and V) wavelengths, consistent with secondary being the cooler star.

Conversely, the primary eclipse is deeper in the B band than the V band and the V band is deeper than the I_c band (see Figures 6 and 7). This again suggests that during the primary eclipse the hotter star is behind the cooler one and more B wavelengths (and V as well) are lost. The PHOEBE fit accounts for this well. The light curves (in all the three filters) are never constant between eclipses, and therefore suggestive of the choice that XZ And is an Algol-type eclipsing binary, which is a semi-detached binary, in which the primary does not fill the Roche Lobe, while the secondary does so exactly. This can clearly be seen in the 3-d models, shown in Figure 5, which were generated in Binary Maker 3 (BM3; Bradstreet and Steelman 2004) using the PHOEBE results. Under these conditions, as shown by both Yang (2013) and Manzoori (2016), mass transfer from the secondary to the primary can and does occur and this explain the overall trend of increasing orbital period.

The agreement between our work and Manzoori (2016) is certainly expected given the fact that we used Manzoori's values for A and q, but this gives us more confidence in our model. It might be worth noting that, according to Pecaut and Mamajek (2013), a typical main sequence A1V has a mass $M_\odot = 2.05$, a radius of approximately $R_\odot = 2.14$, and a surface temperature T = 9300 K. These values are in very good agreement with the fit results, thus indicating that the primary in XZ And is indeed still on the main sequence, while the secondary is further along the evolutionary curve. From the above results, it seems likely that final evolutionary stage of XZ And will be of a main Sequence A star with a helium white dwarf, as the secondary is basically as massive as the Sun and losing mass, but with over twice the radius.

5. Conclusions

The orbital period of the eclipsing binary XZ And is continually evolving due to several mechanisms, which include mass transfer, period modulation due to third body, or bodies, as Demircan *et al.* (1995) suggested, and magnetic effects, as presented by Demircan *et al.* (1995), Yang (2013), and Manzoori (2016).

With the data from the AAVSO International Database, we generated an O–C diagram that seems to agree with the much more extensive dataset from Bob Nelson, albeit only for the last 7,000 cycles or so.

We were successful in using PHOEBE to model XZ And, and the results were in good agreement with previous efforts by Yang (2013) and Manzoori (2016). The fit of T = 9393 K for the primary seems to strengthen the case for the star to be classified as A1V spectral category. Our determination of the B–V value for the secondary agreed overall with the model as well.

The third light parameters we obtained are also in overall agreement with Manzoori (2016), thus indicating the definite possibility of a third body in the system.

XZ And is continuing to prove a very interesting subject. In the paper by Jetsu (2020), the author developed a method to study O–C diagrams of binary systems searching for invisible companions. In the case of XZ And, the author suggests that there are at least ten wide orbiting stars with periods ranging between 1.6 and 91.7 years. More mysteries remain to unravel on XZ And.

6. Acknowledgements

We acknowledge with thanks the variable star observations from the AAVSO International Database contributed by observers worldwide and used in this research. We also wish to thank Dr. M. Pitts and Dr. A. Blose for a careful reading of the manuscript, and Dr. David Bradstreet for considerable help with BM3. Many thanks are also given to the anonymous manuscript referee for his/her extremely helpful comments to improve this work.

References

AAVSO. 2012, VPhot AAVSO photometric software (https://www.aavso.org/vphot).

Applegate, J. H. 1989, *Astrophys. J.*, **337**, 865.

Applegate, J. H. 1992, *Astrophys. J.*, **385**, 621.

Ballesteros, F. J. 2012, *Europhys. Lett.*, **97**, 34008.

Blitzstein, W. 1950, *Astron. J.*, **55**, 165.

Blitzstein, W. 1954, *Astron. J.*, **59**, 251.

Bradstreet, D. H., and Steelman, D. P. 2004, Binary Maker 3, Contact Software (http://www.binarymaker.com).

Castelli, F., and Kurucz, R. L. 2004, arXiv:astro-ph/0405087v1.

Ciocca, M. 2013, *J. Amer. Assoc. Var. Star Obs.*, **41**, 134.

Ciocca, M. 2016, *J. Amer. Assoc. Var. Star Obs.*, **44**, 200.

Demircan, O., Akalin, A., Selam, S., Derman, E., and Mueyesseroglu, Z. 1995, *Astron. Astrophys., Suppl. Ser.*, **114**, 167.

Giuricin, G., Mardirossian, F., and Predolin, F. 1980, *Acta Astron.*, **30**, 561.

Halbedel, E. M. 1984, *Inf. Bull. Var. Stars*, No. 2549, 1.

Jetsu, L. 2020, arXiv:2006.00863v1 [astro-ph.SR].

Manzoori, D. 2016, *Astron. Lett.*, **42**, 329.

Myers, G. 2014, Transform Generator (TG) (https://www.aavso.org/tg).

Pecaut, M. J., and Mamajek, E. E. 2013, *Astrophys. J., Suppl. Ser.*, **208**, 9.

Pleiades Astrophoto, S.L. 2022, PixInsight (https://pixinsight.com/).

Reinhardt, M. W. 1967, *Astron. Nachr.*, **290**, 19.

Schlafly, E. F., and Finkbeiner, D. P. 2011, *Astrophys. J.*, **737**, 103.

Sekiguchi, M., and Fukugita, M. 2000, *Astron. J.*, **120**, 1072.

Shapley, H. 1923, *Bull. Harvard Coll. Obs.*, **790**, 1.

Silvis, G. 2015, Transform Applier (TA) (https://www.aavso.org/ta-release-notes).

Software Bisque. 2018, The Sky X Professional Edition, 10.5.0 (https://www.bisque.com).

Southwest Research Institute (SwRI). 2022, Eclipsing Binaries (http://binaries.boulder.swri.edu/binaries/omc).

University of Iowa Department of Physics and Astronomy. 2017, Imaging the Universe Lab Manual (http://astro.physics.uiowa.edu/ITU/).

Vanmunster, T. 2013, light curve and period analysis software, Peranso v.2.50 (https://www.cbabelgium.com/peranso).

Watson, C., Henden, A. A., and Price, C. A. 2014, AAVSO International Variable Star Index VSX (Watson+, 2006–2014; https://www.aavso.org/vsx).

Wilson, R. E., and Devinney, E. J. 1971, *Astrophys. J.*, **166**, 605.

Wilson, R. E., and Van Hamme, W. 2014, *Astrophys. J.*, **780**, 151.

Yang, Y.-G. 2013, *New Astron.*, **25**, 109.

Zasche, P. 2016, *Open Eur. J. Var. Stars*, **176**. 10.